Supporting Information

Dual-state Fluorescence Emission from Cyanostyrene molecules with multiple nitrogen atoms

Yang Chen,[a] Smruti Ranjan Sahoo,[b,c] Glib V. Baryshnikov,*[b] Lei Gao,*[a,d] Zhijia Zhu[*a]

and Hongwei Wu[*a]

1 Experimental Section

1.1 General methods

Materials: 1H-benzimidazole-2-acetonitrile, 4-pyridine carboxaldehyde, 2-chloro-4-pyridinecarboxaldehyde, 6-quinoline carboxaldehyde, benzaldehyde, lauric acid, and rhodamine B were obtained from Shanghai Hao Hong Biopharmaceutical Technology Co. sodium hydroxide, ethanol, ethyl acetate, dichloromethane, petroleum ether, acetone, tetrahydrofuran, and dimethyl sulfoxide were sourced from Shanghai Titan Technology Co. Column chromatography silica gel was procured from Yantai Jiang you Silicone Development Co. All chemicals and reagents were used without further purification.

Characterizations and instruments:

^{1}H NMR and ^{13}C NMR were conducted using a Bruker 400L spectrometer. High-resolution mass spectrometry data were recorded on a matrix-assisted laser desorption ionization time-off light (MALDI-TOF) mass spectrometer (5800). Absorption spectra were measured with a Shimadzu 1800 spectrophotometer. Fluorescence spectra were recorded using the Horiba FluoroMax-4 from Horiba Scientific. The fluorescent lifetimes were measured with the Edinburgh FLS1000 and Horiba FluoroMax+ spectrofluorometers. The fluorescence quantum yields of solid powders and PMMA doped films were measured using a QM40 with an integrating sphere (φ 150 mm) from Photo Technology International, Inc. (PTI, USA) and a Hamamatsu Photonics C11347-11 with a Quantaurus-QY measurement system, respectively.

1.2 Computational details

The spin-orbit coupling matrix elements (SOCMEs)[1-5] between the energetically lowest triplet states (T_j) and singlet state (S_1) was calculated as root mean squares that

means square root of the sum of squares of spin-orbit coupling matrix elements of all sublevels of the unoccupied states.[6-8] This is given by:

$$\langle S_i | \hat{H}_{SO} | T_j \rangle = \sqrt{\sum_{m=0,\pm1} \langle S_i | \hat{H}_{SO} | T_j^m \rangle^2} \qquad (1)$$

The spin-orbit coupling operator $\hat{H}_{SO}$ was considered in our calculations within the zeroth-order regular approximation (ZORA)[9-12] in accordance with the following expression:

$$\hat{H}_{SO} = \frac{c^2}{(2c^2 - V)^2} \sigma(\nabla V \cdot p), \qquad (2)$$

where σ – Pauli spin matrix vector, p – the linear momentum operator; c – speed of light, V – Kohn−Sham potential.

The intersystem crossing rate constants (k_{ISC}) between the S_1 and T_j states $E(S_1) > E(Tj)$ were estimated using the Plotnikov's simple empirical approximation[13-15]

$$k_{ISC} = k_{S_1 \rightarrow T_j} = 10^{10} \langle S_1 | \hat{H}_{so} | T_j \rangle^2 F_{0m}, \qquad (3)$$

where Franck–Condon factors (F_{0m}) were approximated using the formula:

$$F_{0m} = \sum_n \prod_v \frac{e^{-y} y^{n_v}}{n_v!} \qquad (4)$$

In Equation (4) Huang–Rhys factor y was assumed to be equal to 0.3 and only one average promotive mode $\omega_v = 1400 \, cm^{-1}$ was used when considering $n_v = \Delta E(S_1 - T_j)/\omega_v$. Such a single-mode approximation was considered efficient and accurate enough for the organic dyes and fluorophores.[16-20]

We performed spin-orbit perturbation calculation using the singlet excited state (S_1) optimized geometry to estimate the singlet-triplet $S_1 - T_1$ SOCMEs, and hence k_{ISC} (from Equation 3 and 4), within the TD-DFT/B3LYP/TZP theory level using the quantum chemistry package, ADF 2023.[21] The dichloromethane solvent within the Conductor like Screening Model (COSMO) of solvation was used for solvation matrix effects consideration. The scalar relativistic (SR) orbitals approach was applied to the spin-orbit perturbation.

In the following section, we have discussed the possible two isomer structures of some reported cyanostyrene. To compute the probability of occurrence of one isomer in between the two isomers (Boltzmann population at thermal equilibrium) as a function of temperature (T = 298 K), we calculated the probability of occurrence for the given isomers using the following equation[22, 23]:

$$P(T) = \frac{e^{-\beta \Delta G^K}}{\sum e^{-\beta \Delta G^K}}, \tag{5}$$

where $\beta = {}^1/_{k_B T}$, k_B is the Boltzmann constant and ΔG^K is the Gibbs free energy of the kth isomer.

Neglecting the contributions from the higher excited states, the fluorescence quantum yield (Φ) from the excited state S_1 to the ground state S_0 can be calculated by using the equation[24, 25]:

$$\Phi = \frac{k_r}{k_r + k_{IC} + \sum k_{ISC_i}}, \tag{6}$$

where, k_r and k_{IC} are defined before, and k_{ISC_i} here are the $S_1 \rightarrow T_i$ singlet and energetically lowest triplet states intersystem crossing rate constants. Referring to the Equation (5) and considering the Boltzmann populations (P) for a cyanostyrene compound which possess two possible isomers, the total fluorescence quantum yield (Φ_{tot}) for that compound can be estimated as sum of the fluorescence quantum yield of each kth isomers with their probability of occurrence. This is given as:

$$\Phi_{tot} = \sum \Phi^K P^K \tag{7}$$

All quantum mechanical simulations are performed at a temperature of 298 K.
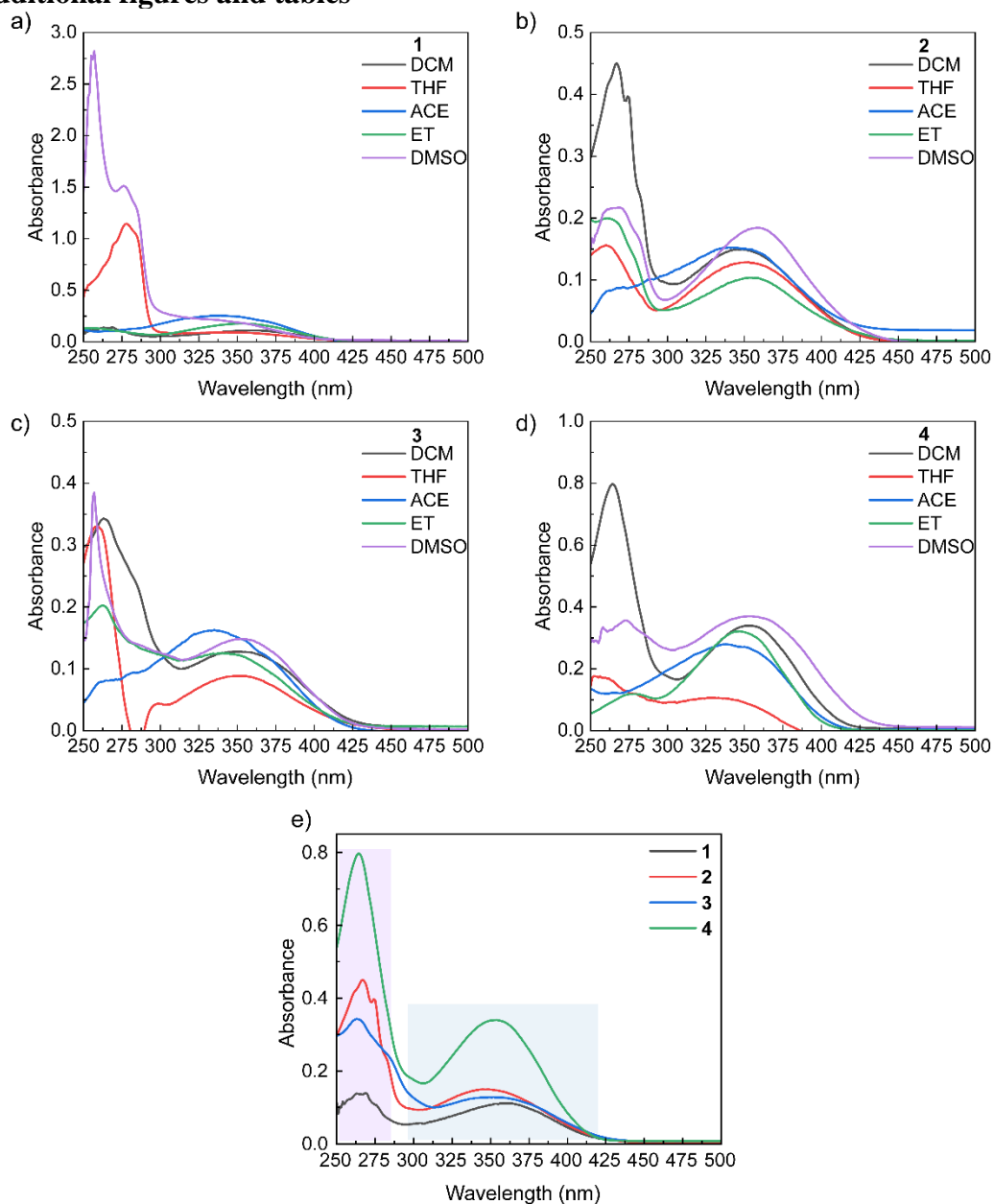
2 Additional figures and tables

Fig. S1. a-d) The UV-vis absorption spectra of compounds **1-4** in five solvents (DCM, THF, ACE, ET and DMSO) at room temperature. e) The UV-vis absorption spectra of compounds **1-4** in DCM at room temperature. The concentration is 100 μM.
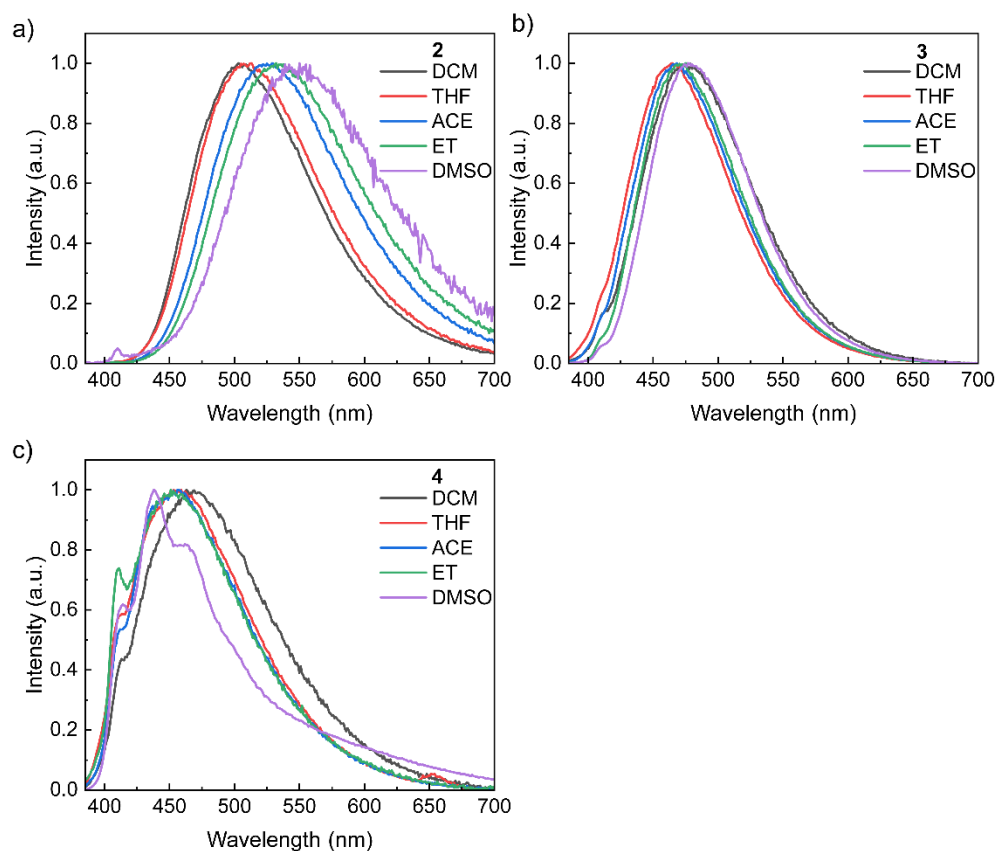
Fig. S2. Normalized emission spectra of compounds **2-4** in five solvents (DCM, THF, ACE, ET and DMSO) at room temperature. The concentration is 100 μM.
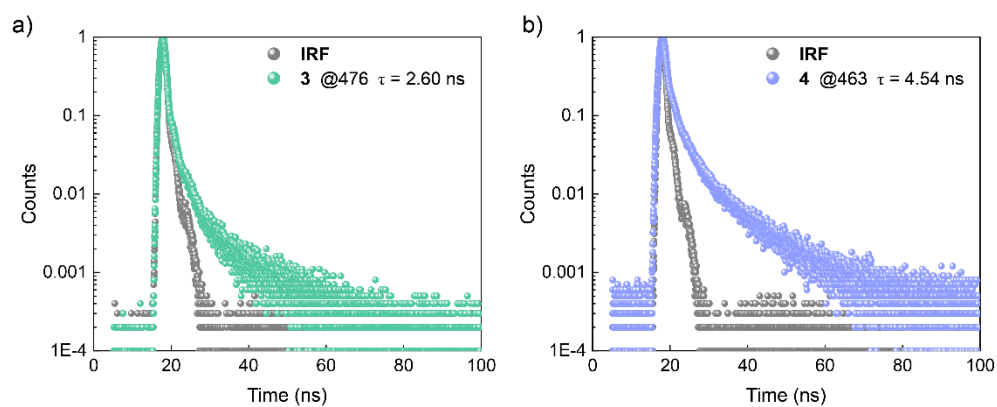

Fig. S3. Lifetime decay profiles of compounds **3** and **4** in DCM (100 μM) under 365 nm excitation.
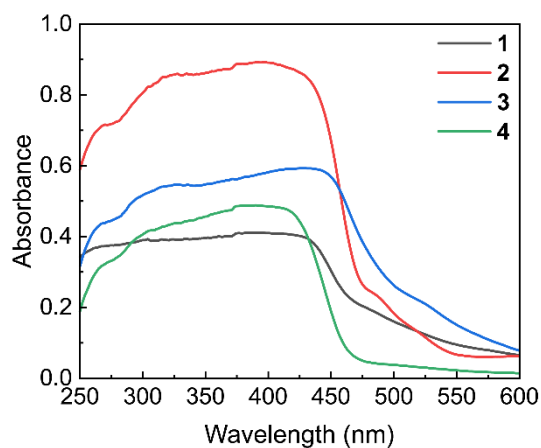
Fig. S4. The UV-vis absorption spectra of compounds **1-4** in powder state.
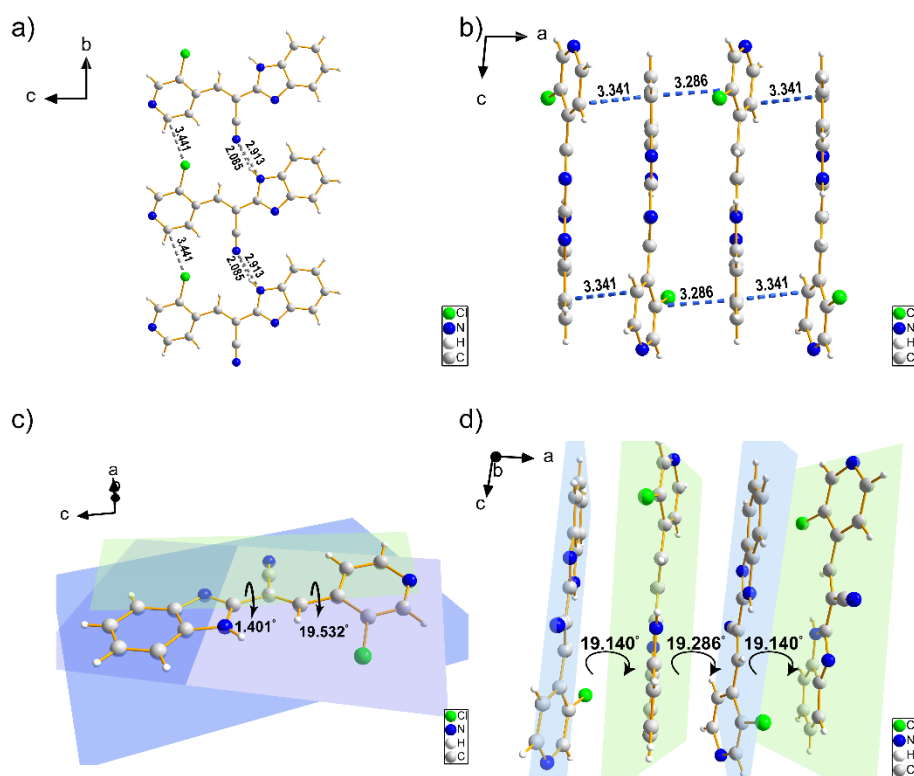
Fig. S5. a) Non covalent bonds in the b-c plane of compound **2** (N-H···N: 2.085 Å; C≡N···N: 2.913 Å and C-Cl···C: 3.441 Å). b) C···C bonds in the a-c plane of compound **2** (3.286 Å and 3.341 Å). c) The dihedral angle between benzimidazole ring and C=C-C≡N (1.401°) and the dihedral angle between 2-chloro-4-pyridine ring and C=C-C≡N (19.532°). d) The dihedral angle between benzimidazole ring and 2-chloro-4-pyridine ring (19.140° and 19.286°)
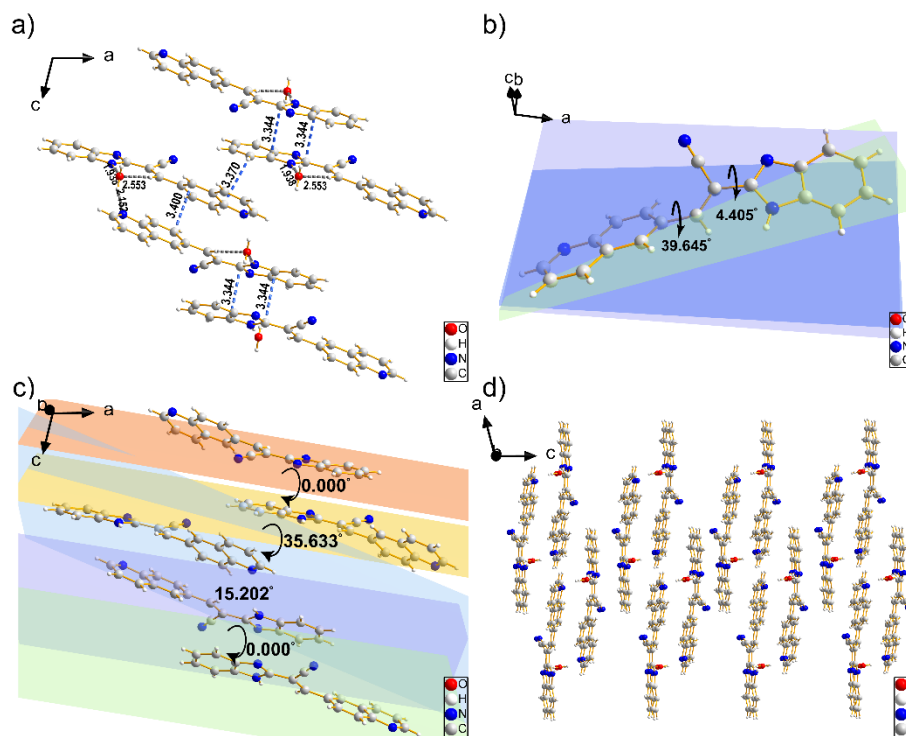
Fig. S6. a) Non covalent bonds in the b-c plane of compound **3** (C···C: 3.344 Å, 3.370 Å and 3.400 Å; N-H···O: 1.938 Å; O-H···N: 2.152 Å and C-H···O: 2.553 Å). b) The dihedral angle between benzimidazole ring and C=C-C≡N (4.405°) and the dihedral angle between 6-quinoline ring and C=C-C≡N (39.645°). c) The dihedral angle between benzimidazole ring 6-quinoline ring (35.633° and 15.202°). d) 2D regular supramolecular tiling pattern in the *a-c* plane of compound **3**.
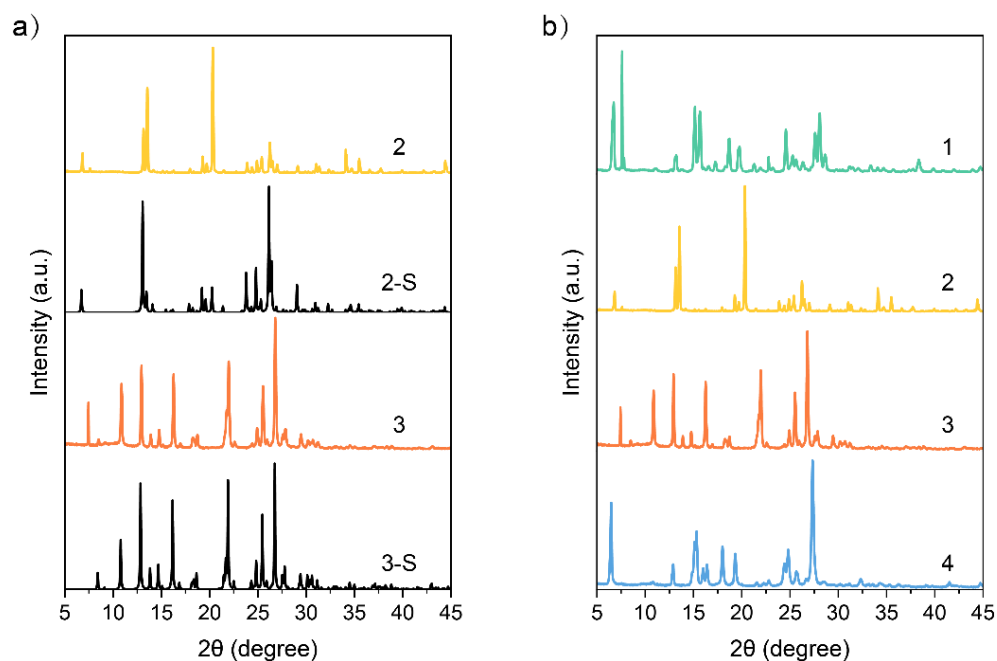
Fig. S7. a) The PXRD spectra of compounds **2** and **3,** alongside their simulated PXRD patterns. b) The PXRD patterns of compounds **1-4**.
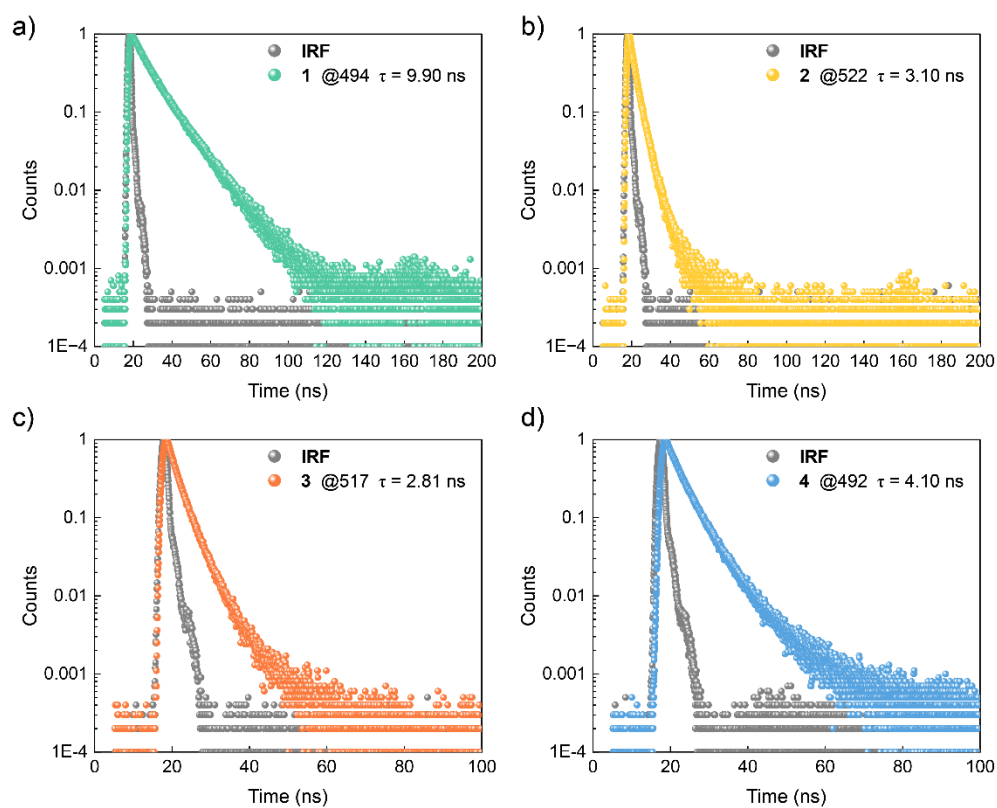

Fig. S8. Lifetime decay profiles of compounds **1-4** in powder state under 365 nm excitation.
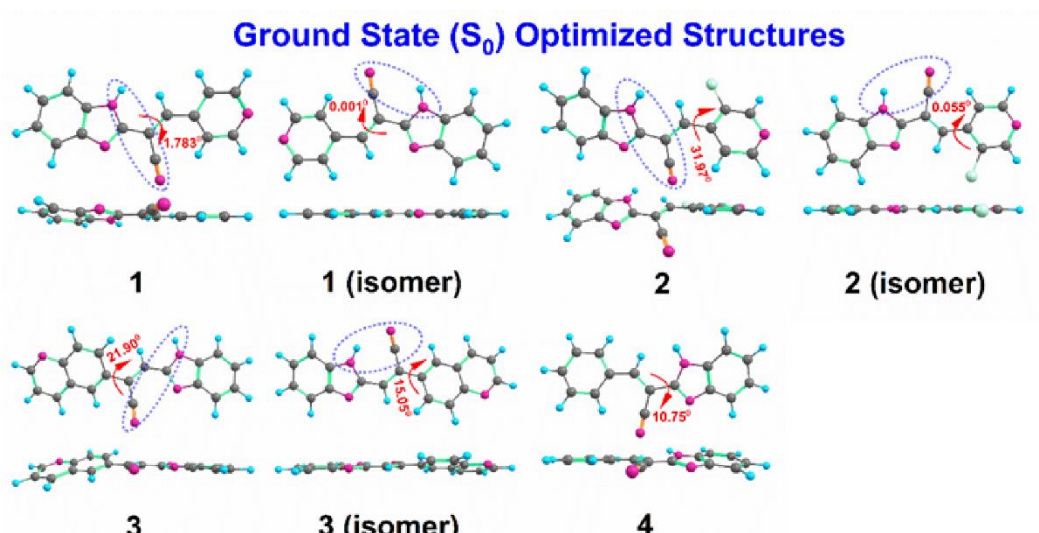
Fig. S9. S_0 optimized DCM solvated geometries of compounds **1-4** with the calculated dihedral angles around C=C/C-C bond at the B3LYP/6-311G (d, p) theory level.
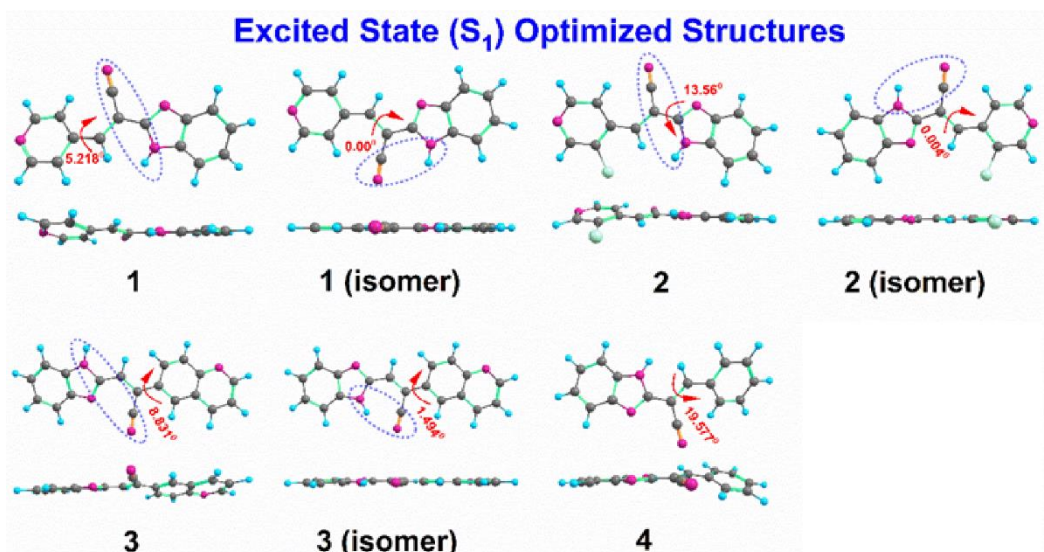

Fig. S10. S_1 optimized DCM solvated geometries of compounds **1-4** with the calculated dihedral angles around C=C/C-C bond at the B3LYP/6-311G (d, p) theory level.
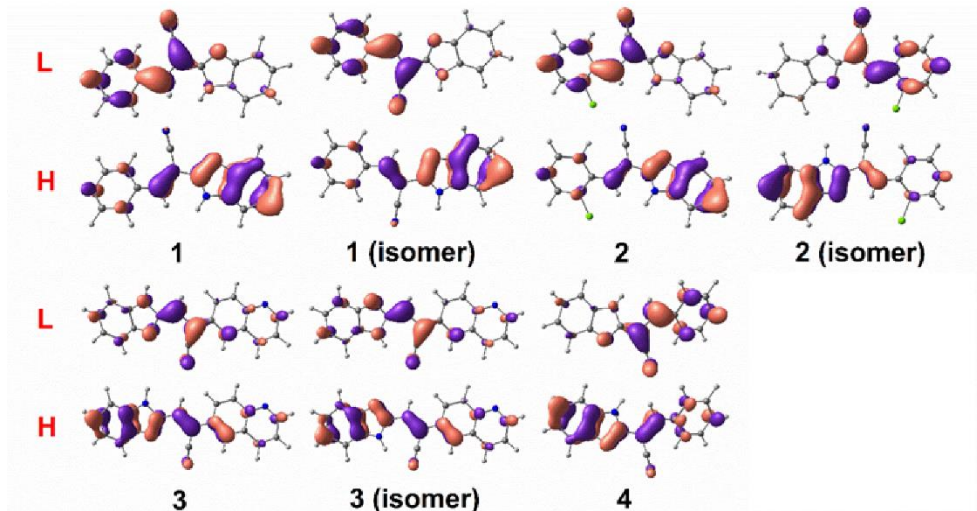
Fig. S11. TD-DFT/B3LYP/6-311G (d, p) theory calculated HOMOs (H) and LUMOs (L) for S_1 excited states ICT distribution for **3** and **4**.
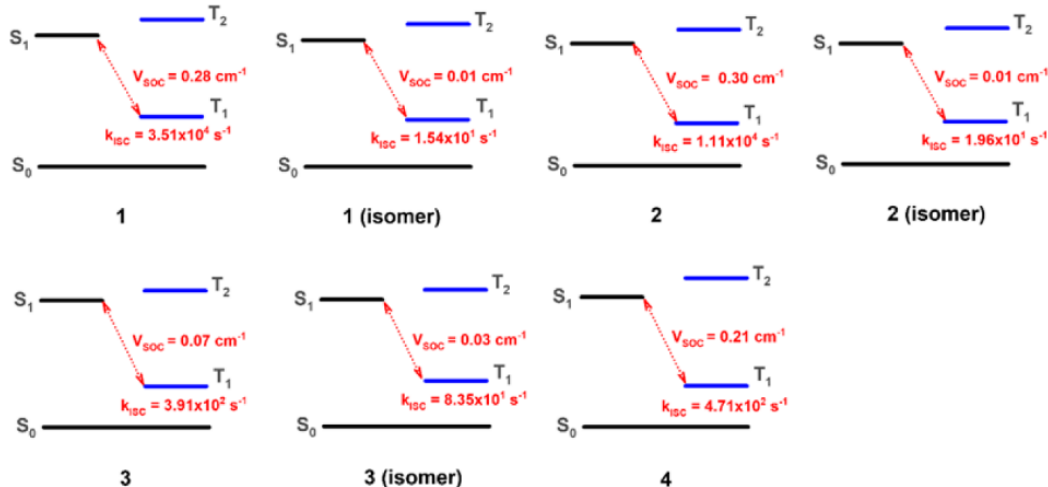

Fig. S12. Schematic representation of calculated singlet-triplet $(S_1 \rightarrow T_1)$ intersystem crossing (k_{ISC}) rates and spin-orbit coupling (V_{SOC}) at room temperature for studied cyanostyrene compounds at TD-DFT/B3LYP/TZP level of theory using ADF 2023 package.
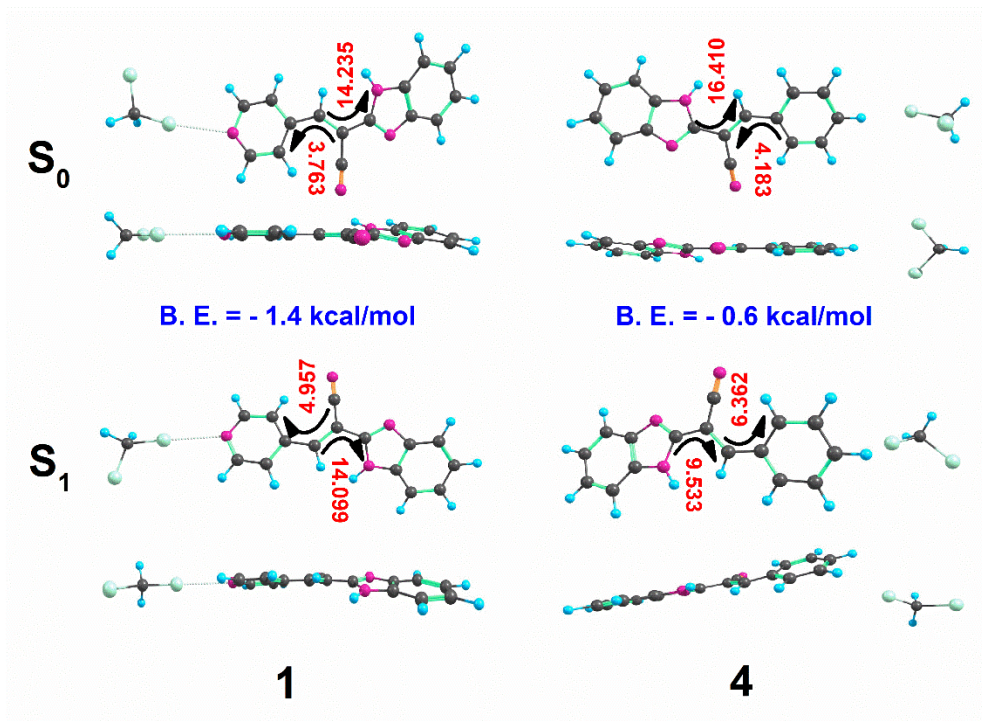
Fig. S13. Calculated S_0 and S_1 state structural confirmation of comp **1** and **4** with DCM molecule. The binding energy for complex structure was calculated and shown for S_0 state.
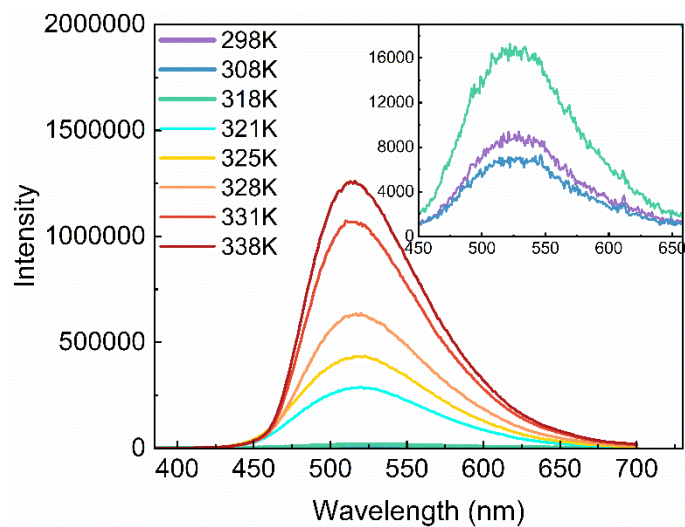

Fig. S14. Emission spectra of compound **1** doped with lauric acid at different temperatures.
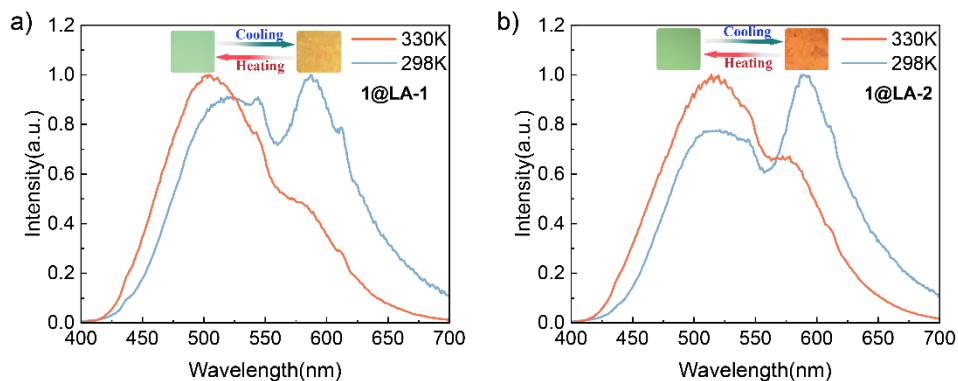
Fig. S15. a) Emission spectra of compound **1@LA-1** at different temperatures. b) Emission spectra of compound **1@LA-2** at different temperatures.
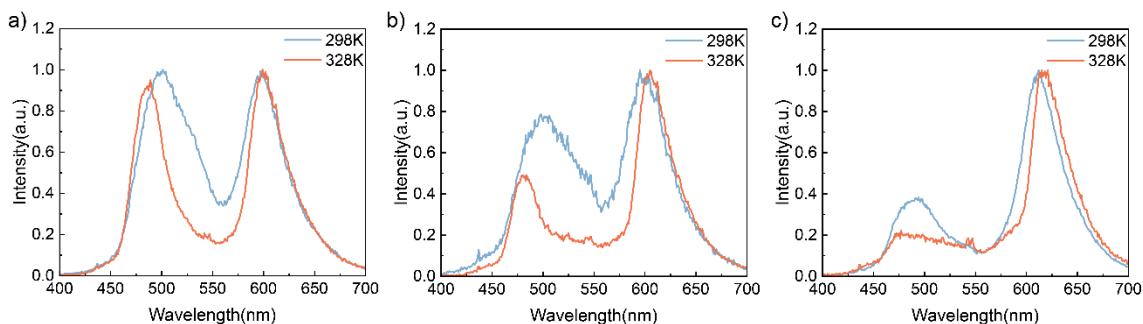

Fig. S16. a) Emission spectra of compound **2@LA-1** (**2: RB**/100:1) at different temperatures. b) Emission spectra of compound **2@LA-2** (**2: RB**/50:1) at different temperatures. c) Emission spectra of compound **2@LA-3** (**2: RB**/10:1) at different temperatures.

Fig. S17. a) Emission spectra of compound **3@LA-1** (**3: RB**/100:1) at different temperatures. b) Emission spectra of compound **3@LA-2** (**3: RB**/50:1) at different temperatures. c) Emission spectra of compound **3@LA-3** (**3: RB**/10:1) at different temperatures.

Fig. S18. a) Emission spectra of compound **4@LA-1** (**4: RB**/100:1) at different temperatures. b) Emission spectra of compound **4@LA-2** (**4: RB**/50:1) at different temperatures. c) Emission spectra of compound **4@LA-3** (**4: RB**/10:1) at different temperatures.
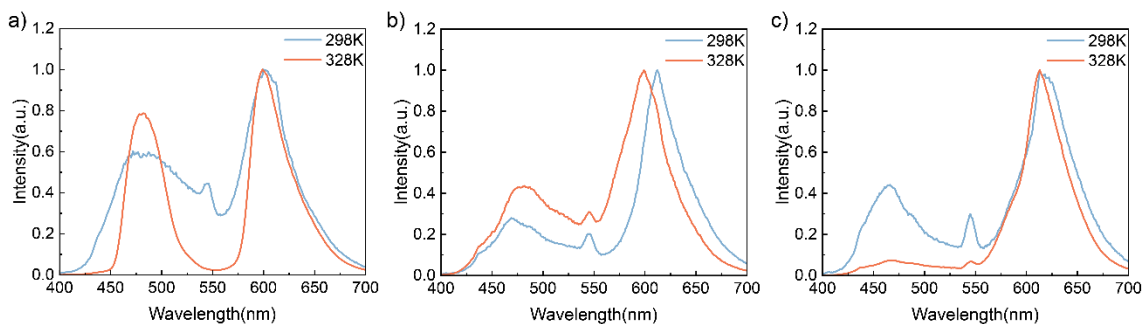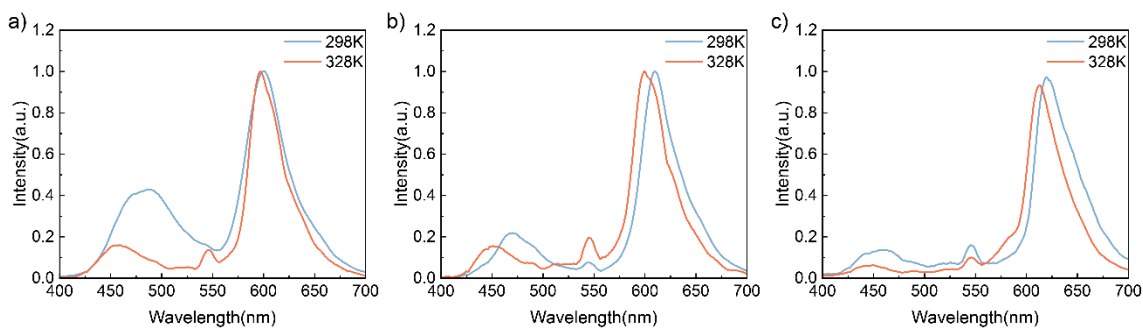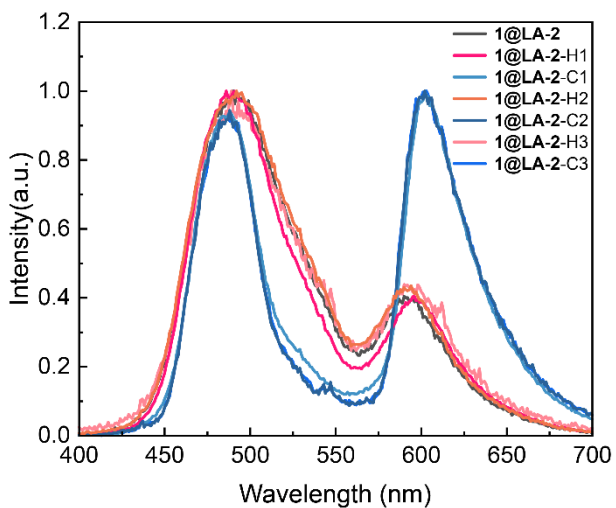

Fig. S19. Normalized emission spectra of **1@LA-2** during 3 cycles.
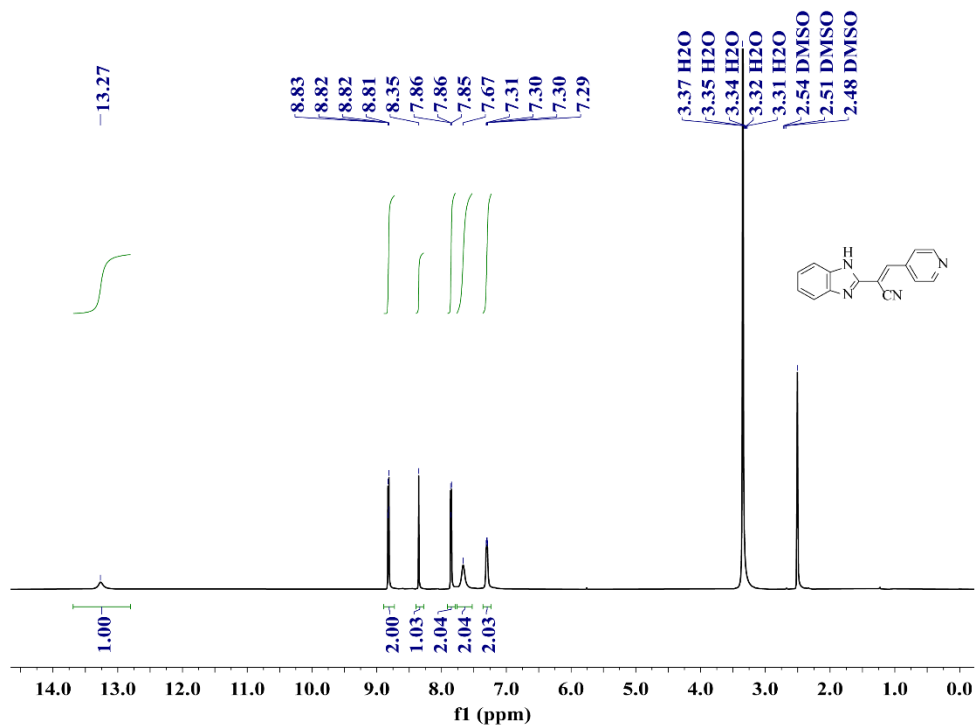
Fig. S20. ^{1}H NMR spectrum of compound **1** in DMSO-d$_6$.
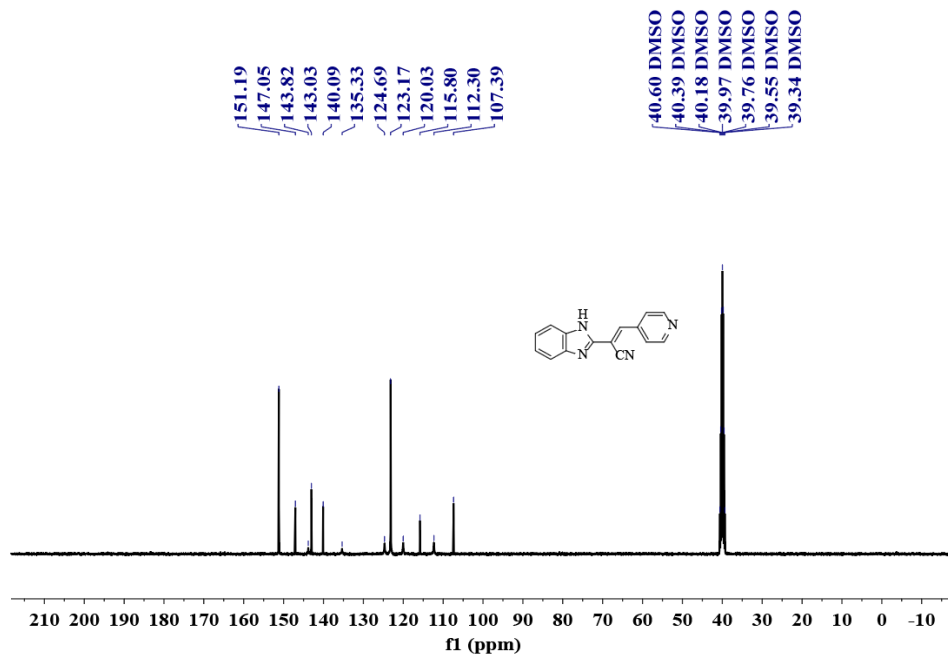
Fig. S21. ^{13}C NMR spectrum of compound **1** in DMSO-d$_6$.
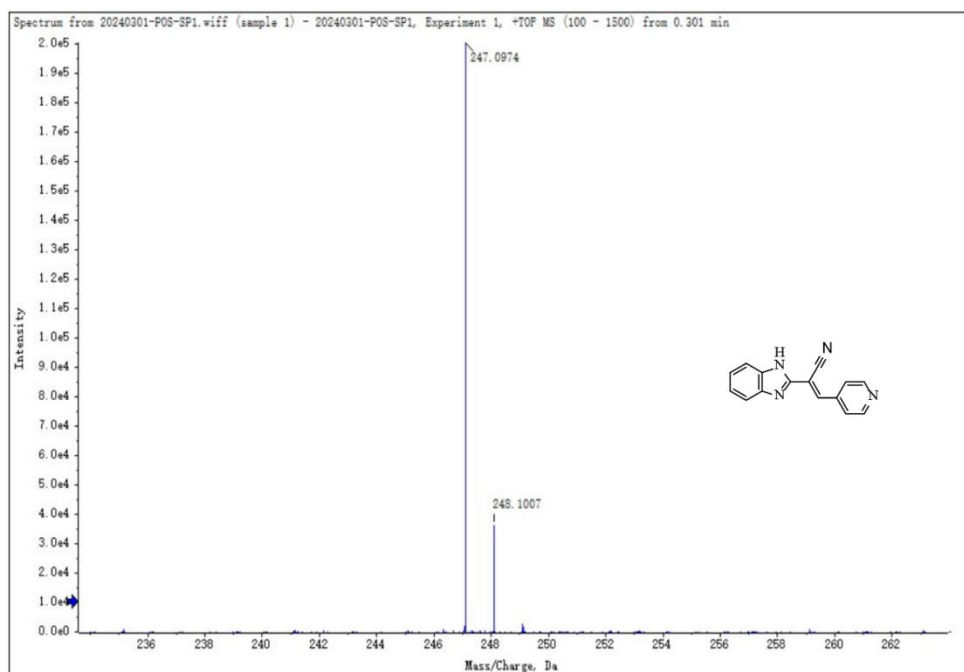
Fig. S22. HRMS Spectrum of compound **1**.
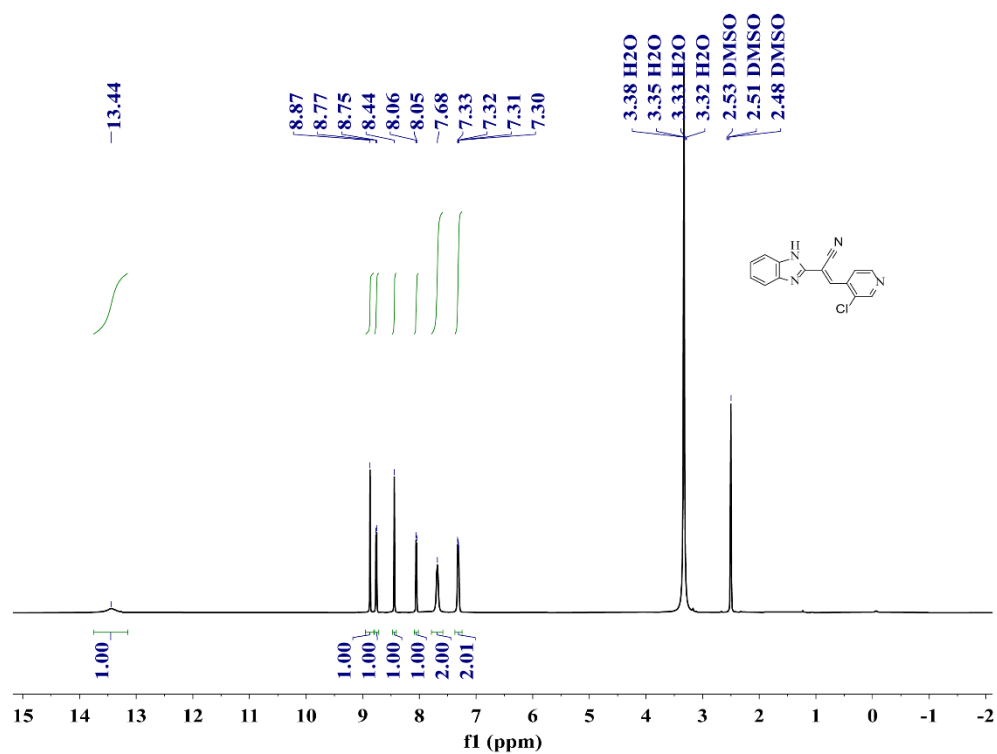
Fig. S23. ^{1}H NMR spectrum of compound **2** in DMSO-d$_6$.
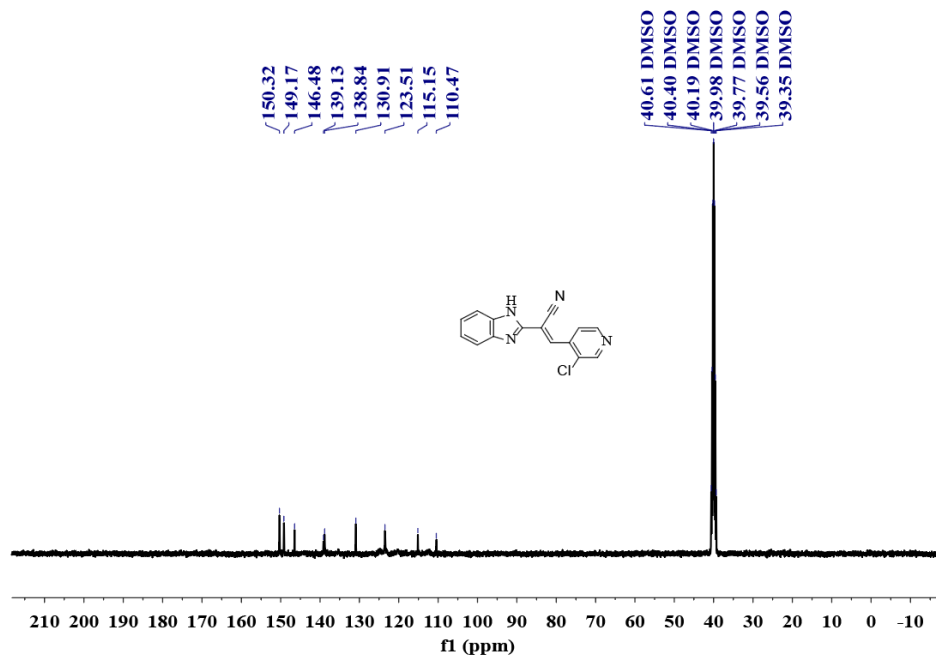
Fig. S24. ^{13}C NMR spectrum of compound **2** in DMSO-d$_6$.
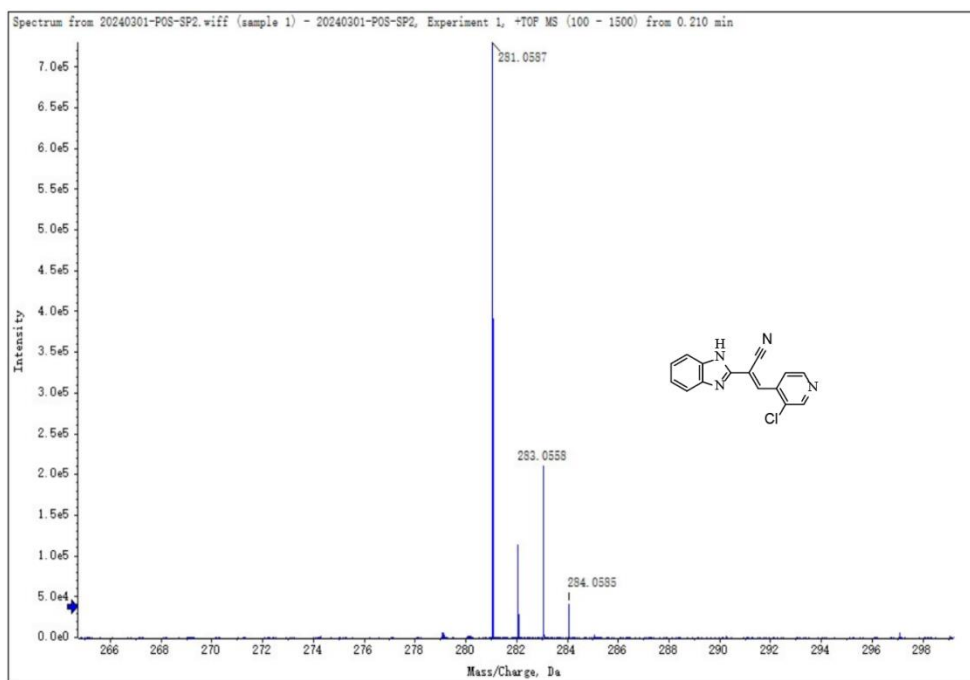
Fig. S25. HRMS Spectrum of compound **2**.
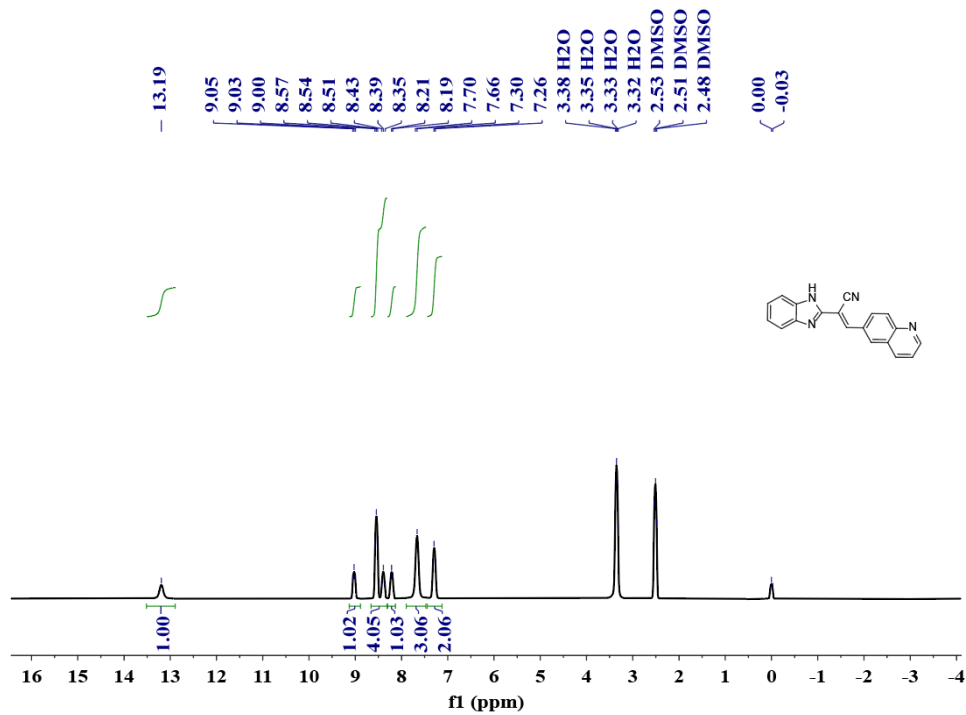
Fig. S26. ^{1}H NMR spectrum of compound **3** in DMSO-d$_6$.
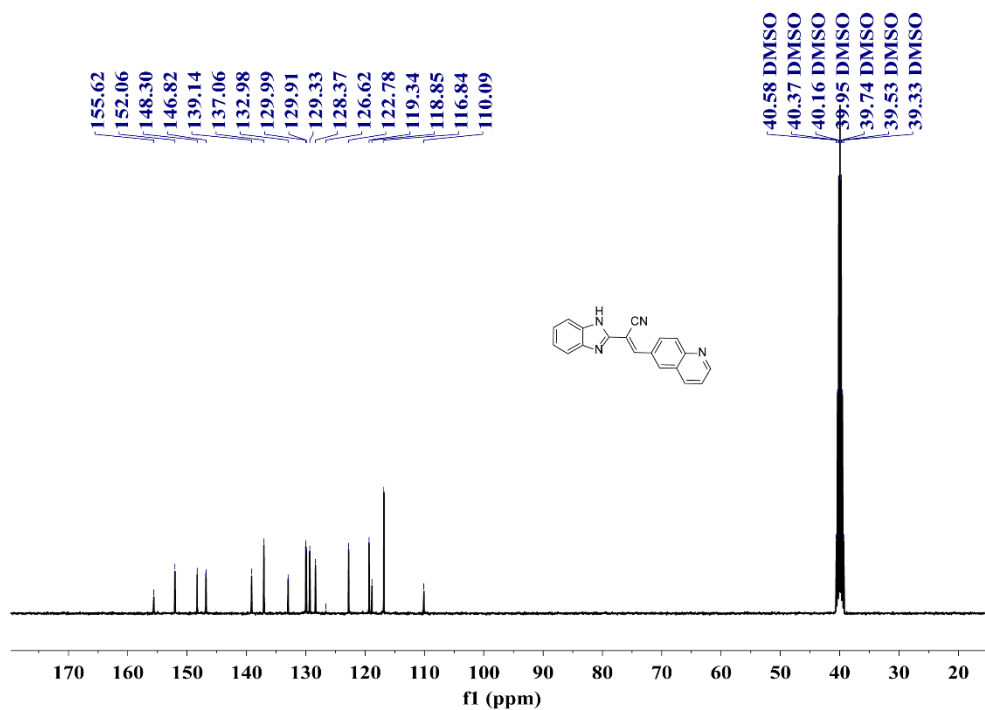
Fig. S27. ^{13}C NMR spectrum of compound **3** in DMSO-d$_6$.
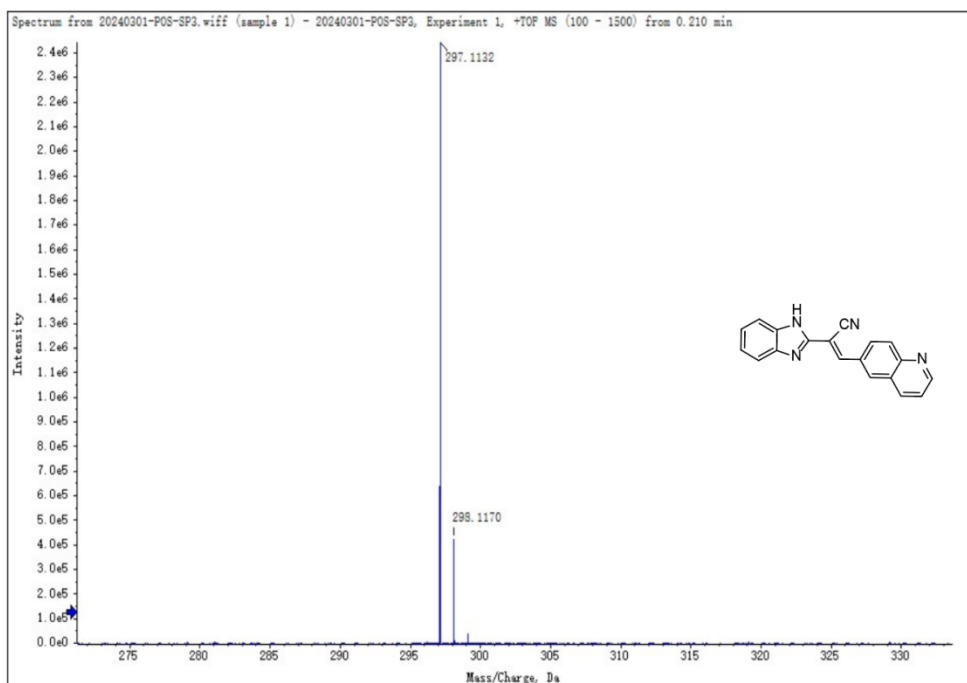
Fig. S28. HRMS Spectrum of compound **3**.
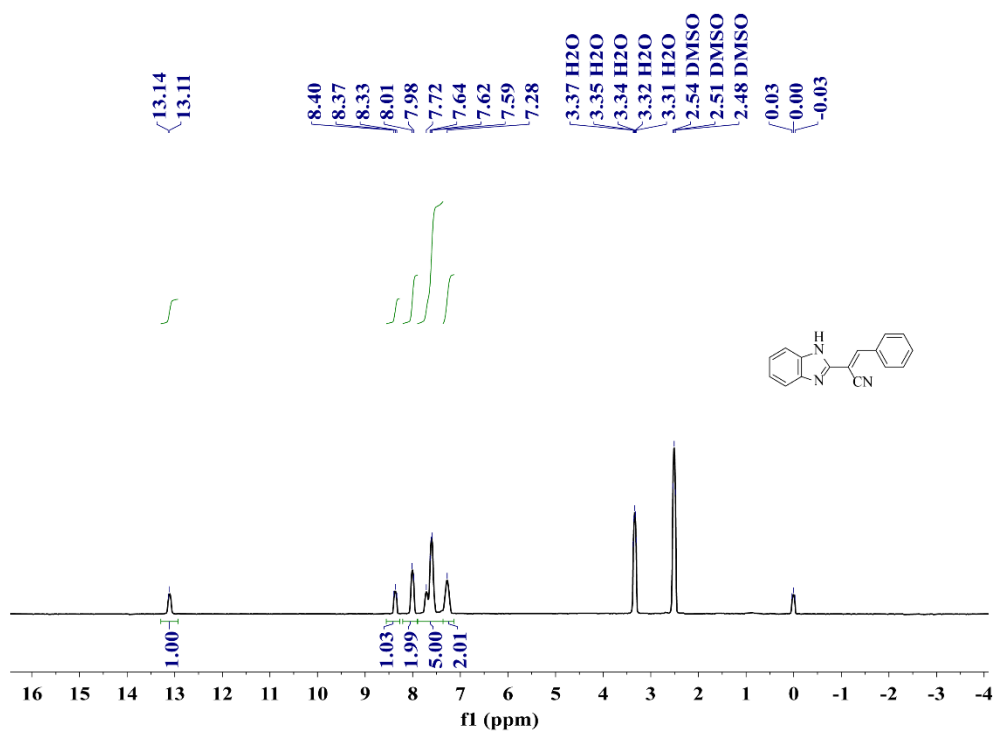
Fig. S29. ^{1}H NMR spectrum of compound **4** in DMSO-d$_6$.
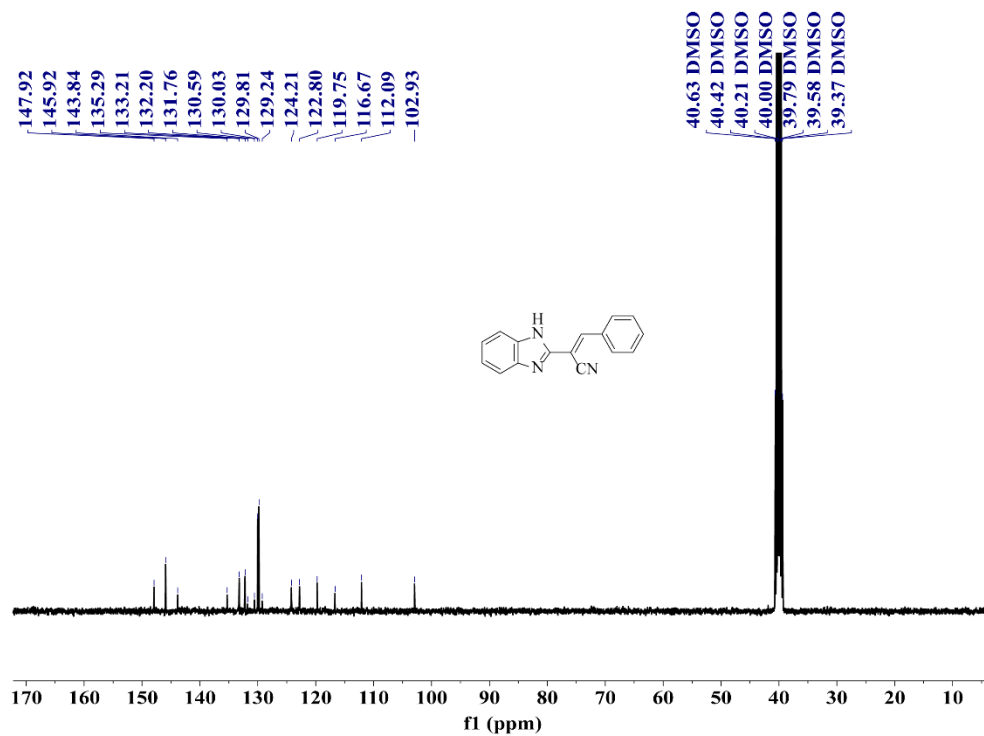
Fig. S30. ^{13}C NMR spectrum of compound **4** in DMSO-d$_6$.
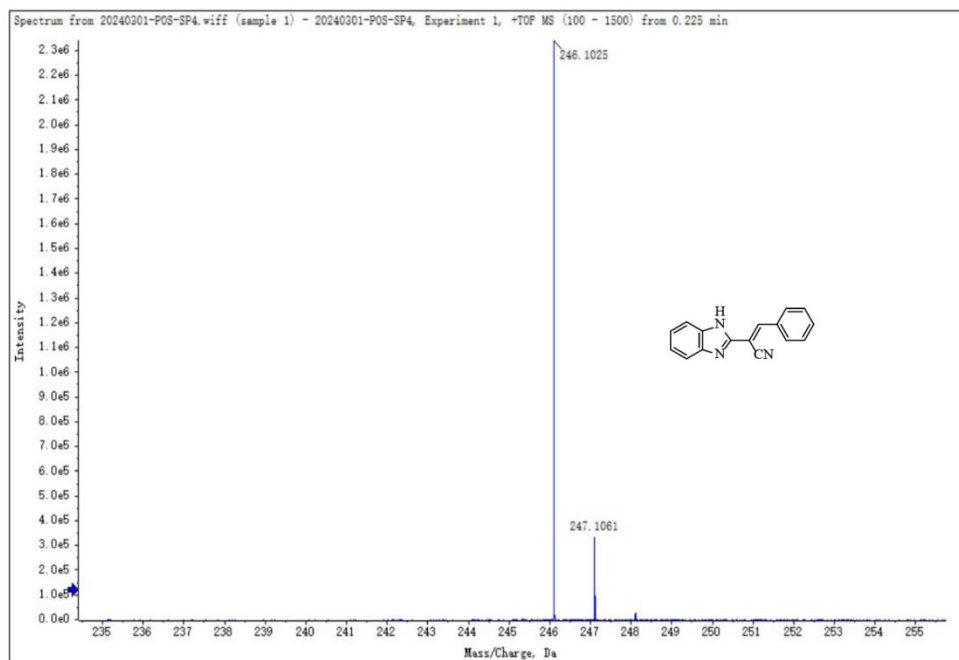
Fig. S31. HRMS Spectrum of compound **4**.
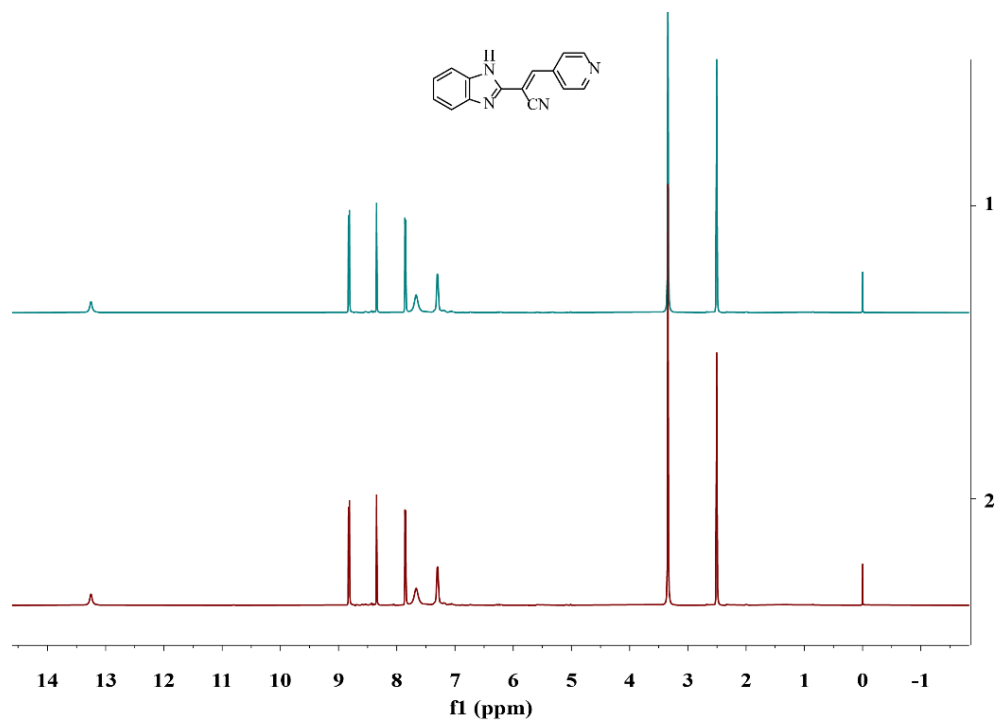
Fig. S32. ¹H NMR spectrum of compound **1** before (upper)) and after (lower) exposure to 365 nm UV light in DMSO-d₆.
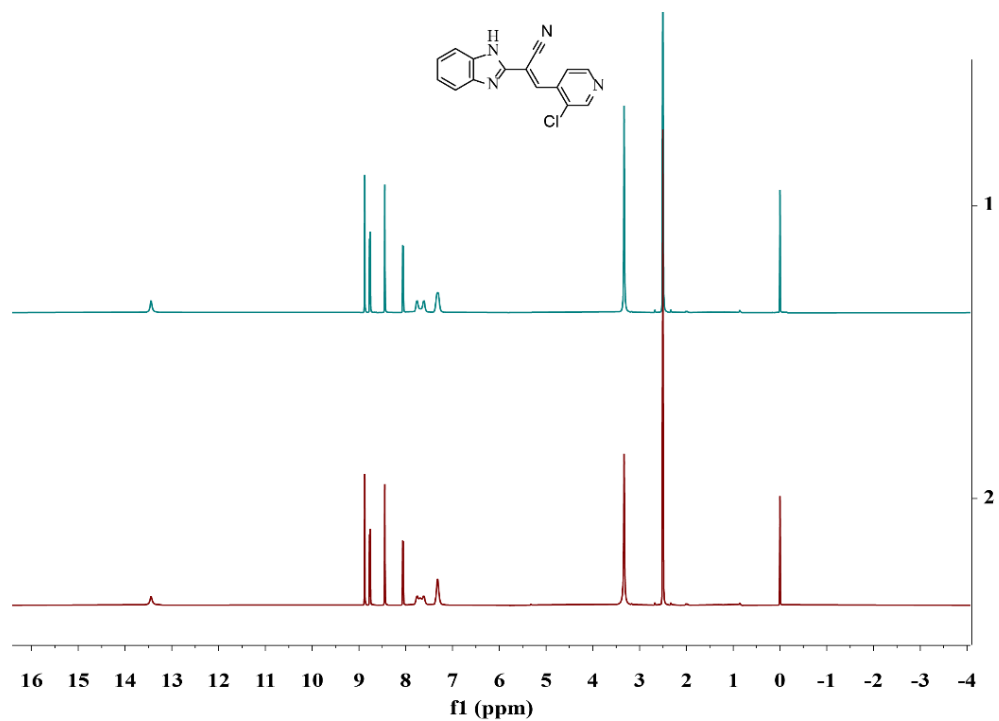
Fig. S33. ¹H NMR spectrum of compound **2** before (upper)) and after (lower) exposure to 365 nm UV light in DMSO-d₆.
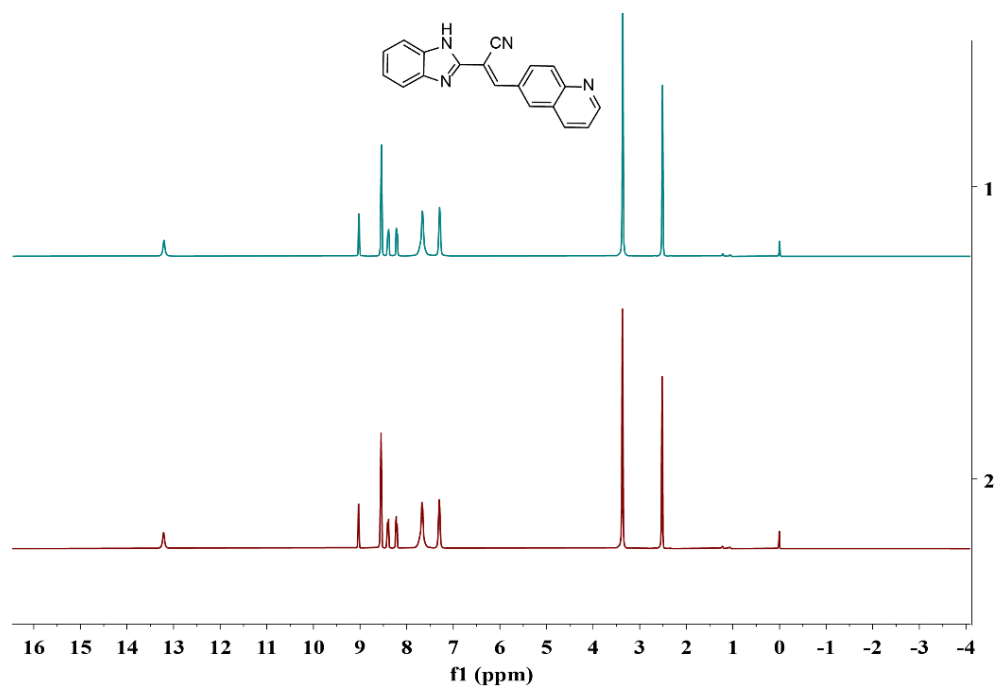
Fig. S34. ^{1}H NMR spectrum of compound **3** before (upper)) and after (lower) exposure to 365 nm UV light in DMSO-d$_6$.
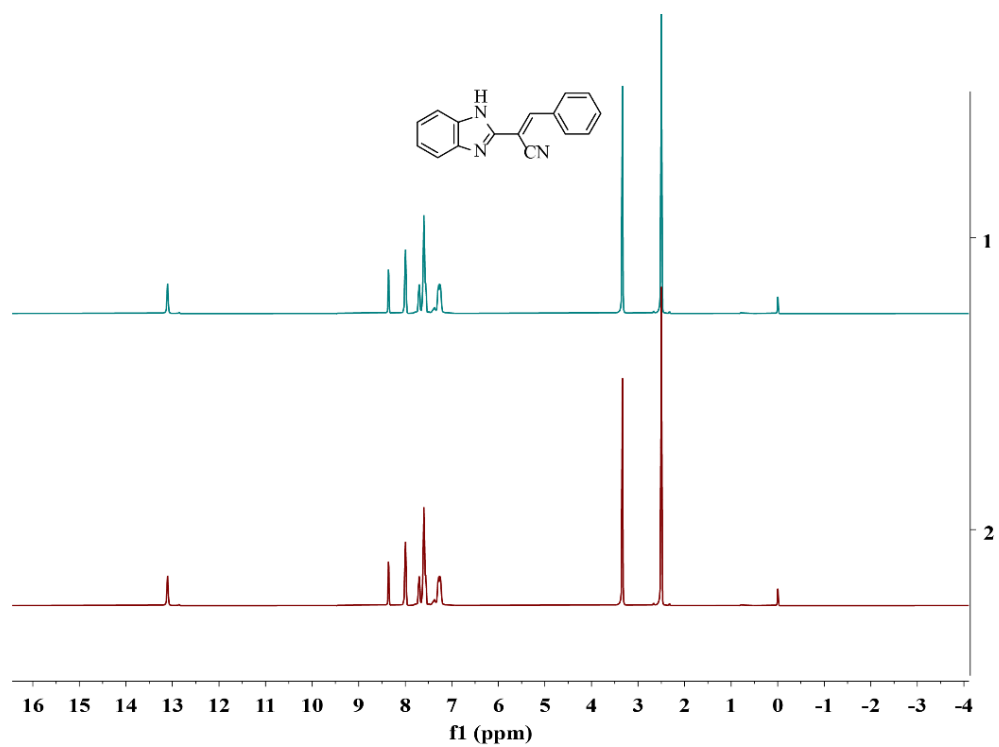
Fig. S35. ^{1}H NMR spectrum of compound **4** before (upper)) and after (lower) exposure to 365 nm UV light in DMSO-d$_6$.

Table S1. Crystallographic parameters of compounds **2** and **3**.

Identification	**2**	**3**
Empirical formula	$C_{15}H_9ClN_4$	$C_{19}H_{14}N_4O$
Formula weight	280.71	314.34
Crystal system	monoclinic	monoclinic
Space group	I 12/a1	P 121/c1
a/Å	13.6775(8)	10.8369(8)
b/Å	7.0104(3)	7.3671(7)
c/Å	26.4013(12)	20.0273(14)
α/°	90	90
β/°	95.209(5)	104.078(7)
γ/°	90	90
Volume/Å^3	2521.0(2)	1550.9(2)
Z	8	4
ρ_{calc}/(g/cm^3)	1.479	1.346
CCDC	2355948	2355949

Table S2. Photophysical data of compounds **1-4** in solution state and powder state.

Compounds	1	2	3	4
$\lambda_{abs, max}$ (nm) in DCM	262	266	263	264
$\lambda_{em, max}$ (nm) in DCM	496	503	476	463
Fluorescence lifetime (ns) in DCM	2.48	5.54	2.60	4.54
Quantum yield (%) in DCM	42.7	35.5	0.3	0.2
Quantum yield (%) in THF	21.0	38.3	1.0	0.5
Quantum yield (%) in ACE	28.3	32.3	0.9	0.8
Quantum yield (%) in ET	28.5	19.2	1.0	0.3
Quantum yield (%) in DMSO	12.7	4.0	3.7	1.8
k_r (s^{-1}) in DCM	1.72×10^8	6.41×10^7	1.15×10^6	4.41×10^5
k_{nr} (s^{-1}) in DCM	2.31×10^8	1.16×10^8	3.83×10^8	2.20×10^8
$\lambda_{em, max}$ (nm)	494	522	517	492
Fluorescence lifetime (ns)	9.90	3.10	2.81	4.10
Quantum yield (%)	27.4	8.0	26.6	11.2
k_r (s^{-1})	2.77×10^7	2.58×10^7	7.01×10^7	5.15×10^7
k_{nr} (s^{-1})	7.33×10^7	2.97×10^8	2.82×10^8	1.85×10^8

Table S3. TD-DFT/B3LYP/6-311G (d, p) theory calculated $S_1 \rightarrow S_0$ fluorescence emission wavelengths, energies, and corresponding oscillator strength values for compounds **1-4** in gas phase and DCM solvated medium.

Compounds	Medium	λ (nm)	E (eV)	Osc. strength (f)	Expt (nm) in DCM
1	Gas phase	482	2.57	0.0770	
	DCM	489	2.53	1.0757	
1 (isomer)	Gas phase	491	2.52	0.2600	496
	DCM	522	2.38	0.7062	
2	Gas phase	510	2.43	0.0558	
	DCM	508	2.44	1.0232	
2 (isomer)	Gas phase	513	2.42	0.2223	503
	DCM	545	2.27	0.6628	
3	Gas phase	438	2.83	1.0870	
	DCM	506	2.45	1.6058	
3 (isomer)	Gas phase	428	2.90	1.2776	476
	DCM	496	2.50	1.7167	
4	Gas phase	458	2.71	0.2347	
	DCM	502	2.47	1.1335	463

Table S4. Calculated radiative rate (k_r), internal conversion rate (k_{IC}) constants (at adiabatic excitation energy) using TVCF formalism with DRE approach. Calculated probability of occurrence ($P(T)$), and fluorescence quantum yields (Φ_{tot}^{theory}) which further compared to the experimental quantum yield in dichloromethane solvent.

Compounds	k_r (s^{-1})	k_{IC} (s^{-1})	P(T)	Φ^{theory}(%)	Φ_{tot}^{theory}(%)	Expt. Φ_{DCM}(%)
1	2.146×10^8	1.450×10^9	0.458	12.9	59.5	42.7
1 (isomer)	1.496×10^8	1.715×10^6	0.542	98.9		
2	5.373×10^7	9.371×10^{10}	0.125	0.06	85.7	35.5
2 (isomer)	1.314×10^8	2.875×10^6	0.875	97.9		
3	1.091×10^8	8.367×10^{10}	0.450	0.13	0.22	0.3
3 (isomer)	1.840×10^8	6.099×10^{10}	0.550	0.30		
4	6.596×10^7	5.636×10^{10}	--	0.12	0.12	0.2

Table S5. Calculated total energies and energy differences of studied isomeric compounds.

Compounds	Total energy E ($kcal/mol$)	Energy difference ($kcal/mol$)
1	-500005.4362	1.8492
1 (isomer)	-500007.2855	
2	-788419.6445	1.2322
2 (isomer)	-788420.8767	
3	-596443.0086	1.5261
3 (isomer)	-596444.5347	

Table S6. Summarizes the experimental (EX) and computationally (COMP) obtained photophysics data.

Compounds	1	2	3	4
$\lambda_{em,\ max}$ (nm) in DCM of EX	496	503	476	463
$\lambda_{em,\ max}$ (nm) in DCM of COMP	489	508	506	502
Quantum yield (%) in DCM of EX	42.7	35.5	0.3	0.2
Quantum yield (%) in DCM of COMP	59.5	85.7	0.22	0.12
k_r (s^{-1}) in DCM of EX	1.72×10^8	6.41×10^7	1.15×10^6	4.41×10^5
k_r (s^{-1}) in DCM of COMP	2.146×10^8	5.373×10^7	1.091×10^8	6.596×10^7

References

(1) M. J. Frisch, G. W. T., H. B. Schlegel, G. E. Scuseria, M. A. Robb, J. R. Cheeseman, G. Scalmani, V. Barone, G. A. Petersson, H. Nakatsuji, X. Li, M. Caricato, A. V. Marenich, J. Bloino, B. G. Janesko, R. Gomperts, B. Mennucci, H. P. Hratchian, J. V. Ortiz, A. F. Izmaylov, J. L. Sonnenberg, D. Williams-Young, F. Ding, F. Lipparini, F. Egidi, J. Goings, B. Peng, A. Petrone, T. Henderson, D. Ranasinghe, V. G. Zakrzewski, J. Gao, N. Rega, G. Zheng, W. Liang, M. Hada, M. Ehara, K. Toyota, R. Fukuda, J. Hasegawa, M. Ishida, T. Nakajima, Y. Honda, O. Kitao, H. Nakai, T. Vreven, K. Throssell, J. A. Montgomery, Jr., J. E. Peralta, F. Ogliaro, M. J. Bearpark, J. J. Heyd, E. N. Brothers, K. N. Kudin, V. N. Staroverov, T. A. Keith, R. Kobayashi, J. Normand, K. Raghavachari, A. P. Rendell, J. C. Burant, S. S. Iyengar, J. Tomasi, M. Cossi, J. M. Millam, M. Klene, C. Adamo, R. Cammi, J. W. Ochterski, R. L. Martin, K. Morokuma, O. Farkas, J. B. Foresman and D. J. Fox, Gaussian, Inc., Wallingford CT, 2016. Gaussian 16, Revision B.01. **2016**.

(2) M. E. Casida, C. Jamorski, K. C. Casida, D. R. Salahub, *J. Chem. Phys.,* 1998, **108**, 4439-4449.

(3) A. D. Laurent, C. Adamo, D. Jacquemin, *Phys. Chem. Chem. Phys.,* 2014, **16**, 14334-14356.

(4) C. Adamo, D. Jacquemin, *Chem. Soc. Rev.,* 2013, **42**, 845-856.

(5) L. A. Curtiss, M. P. McGrath, J. P. Blaudeau, N. E. Davis, R. C. Binning Jr, L. Radom, *J. Chem. Phys.,* 1995, **103**, 6104-6113.

(6) P. K. Samanta, D. Kim, V. Coropceanu, J.-L. Brédas, *J. Am. Chem. Soc.,* 2017, **139**, 4042-4051.

(7) A. D. McLean, G. S. Chandler, *J. Chem. Phys.,* 1980, **72**, 5639-5648.

(8) Y. Niu, W. Li, Q. Peng, H. Geng, Y. Yi, L. Wang, G. Nan, D. Wang, Z. Shuai, *Mol. Phys.,* 2018, **116**, 1078-1090.

(9) E. Van Lenthe, J. G. Snijders, E. J. Baerends, *J. Chem. Phys.,* 1996, **105**, 6505-6516.

(10) Q. Peng, Y. Yi, Z. Shuai, J. Shao, *J. Am. Chem. Soc.,* 2007, **129,** 9333-9339.

(11) Y. L. Niu, Q. Peng, Z. G. Shuai, *Sci. China Ser. B,* 2008, **51**, 1153-1158.

(12) E. Van Lenthe, R. Van Leeuwen, E. J. Baerends, J. G. Snijders, *Int. J. Quantum. Chem.,* 1996, **57**, 281-293.

(13) V. G. Plotnikov, *Int. J. Quantum. Chem.,* 1979, **16**, 527-541.

(14) Z. Shuai, Q. Peng, *Natl. Sci. Rev.,* 2017, **4**, 224-239.

(15) Y. Niu, Q. Peng, C. Deng, X. Gao, Z. Shuai, *J. Phys. Chem. A,* 2010, **114**, 7817-7831.

(16) R. R. Valiev, A. N. Sinelnikov, Y. V. Aksenova, R. T. Kuznetsova, M. B. Berezin, A. S. Semeikin, V. N. Cherepanov, *Spectrochim. Acta. A,* 2014, **117**, 323-329.

(17) R. R. Valiev, R. T. Nasibullin, V. N. Cherepanov, G. V. Baryshnikov, D. Sundholm, H. Ågren, B. F. Minaev, T. Kurtén, *Phys. Chem. Chem. Phys.,* 2020, **22**, 22314-22323.

(18) R. R. Valiev, R. T. Nasibullin, V. N. Cherepanov, A. Kurtsevich, D. Sundholm, T. Kurtén, *Phys. Chem. Chem. Phys.,* 2021, **23,** 6344-6348.

(19) R. R. Valiev, B. S. Merzlikin, R. T. Nasibullin, A. Kurtzevitch, V. N. Cherepanov, R. R. Ramazanov, D. Sundholm, T. Kurtén, *Phys. Chem. Chem. Phys.,* 2023, **25**, 6406-6415.

(20) R. Englman, J. Jortner, *Mol. Phys.,* 1970, **18**, 145-164.

(21) *ADF* Theoretical Chemistry, Vrije Universiteit, Amsterdam, The Netherlands, 2023. http://www.scm.com (Accessed.)

(22) C. E. Buelna-Garcia, J. L. Cabellos, J. M. Quiroz-Castillo, G. Martinez-Guajardo, C. Castillo-Quevedo, A. de-Leon-Flores, G. Anzueto-Sanchez, M. F. Martin-del-Campo-Solis, *Materials* 2020, **14,** 112.

(23) E. W. Schlag, S. Schneider, S. F. Fischer, *Annu. Rev. Phys. Chem.,* 1971, **22**, 465-526.

(24) S. P. McGlynn, T. Azumi, M. Kinoshita, *Prentice-Hall*, 1969.

(25) W. Siebrand, *J. Chem. Phys.,* 1967, **46**, 440-447.